# Electrooxidation of CO and CO/$H_2$ mixtures on a Pt–Sn catalyst prepared by an implantation method

N.M. Marković *, A. Widelôv, P.N. Ross

*Material Sciences Division, Lawrence Berkeley National Laboratory, University of California, Berkeley, CA 94720, USA*

O.R. Monteiro and I.G. Brown

*Accelerator and Fusion Research Division, Lawrence Berkeley National Laboratory, University of California, Berkeley, CA 94720, USA*

Received 13 August 1996; accepted 1 November 1996

A new type of ion implantation technique is used to create a non-equilibrium Pt–Sn(IMP) near-surface alloy with ca. 8.6 at% Sn. The surface composition was determined by low-energy ion-scattering (LEIS). The kinetics of the electrooxidation of CO and 2% CO/$H_2$ mixtures on Pt–Sn(IMP) is essentially identical to that of $Pt_3Sn(110)$. The fact that any non-equilibrium composition can be easily prepared by this implantation method opens an interesting practical opportunity to create a new Pt–Sn alloy fuel cell catalyst having an otherwise unobtainable surface composition of Sn. This method also appears to have general utility in alloy catalysis as a means of exploring compositions in thermodynamically unfavorable regions of the bulk phase diagram.

**Keywords:** electrocatalysis, carbon monoxide, platinum–tin alloy, implantation, electrooxidation

## 1. Introduction

Decades before the terms "nanoscale materials" or "nanoscale engineering" were coined, catalytic chemists realized that materials with unique properties were created by bringing two or more different metals together at the molecular level. In electrocatalysis, the activity and stability of solid solutions of metals (alloys) have been widely explored. Hoping that the combination of different metals would have superior catalytic activity and/or stability relative to the pure metals, the electrooxidation of potential fuels for fuel cells was extensively studied on different bimetallic systems [1–13]. Of the various systems examined, bimetallic $Pt_3Sn$ alloys are of particular interest because this system exhibits a remarkably high catalytic activity for the electrooxidation of CO and CO/$H_2$ mixtures, e.g. more than four orders of magnitude more active than pure Pt [14,15]. Another interesting feature of this alloy is that the catalytic activity of the $Pt_3Sn(hkl)$ surfaces for CO oxidation is also strongly dependent on the surface geometry, with the onset potential being lower by $\sim 0.13$ V on the annealed (111) versus the sputtered (110) surface, both surfaces having a composition of 20–25 at% Sn. We have postulated that the uniquely high activity of $Pt_3Sn$ surfaces is due to the creation of a unique state of $CO_{ad}$ adsorbed on Pt sites adjacent to Sn atoms (weakly bonded $CO^{w}_{ad}$), and to the ability of Sn atoms to activate water (probably to $OH_{ad}$) at low overpotentials, i.e. a subtle variation to the classical bifunctional mechanism of electrocatalytic oxidation [7]. However, recent theoretical calculations by Anderson and co-workers [16] indicate Sn atoms in a Pt lattice do not activate water at low potentials. It is clear that the mechanism of CO oxidation on these surfaces, especially the mechanism of action of Sn atoms in the surface, warrants much further study.

A detailed examination of the role of Sn in the oxidation of CO and CO/$H_2$ mixtures on Pt–Sn surfaces faces a fundamental limitation imposed by both the bulk and surface thermodynamics of the Pt–Sn system. The bulk phase diagram [17] indicates that in the Pt-rich end there are no single-phase alloys between the solid solution limit, which is not well known but suggested to be about 5 at% Sn, and the intermetallic phase $Pt_3Sn$. A similar thermodynamic limitation exists for a number of other Pt–group IV alloys which are of interest. The surface thermodynamics of Pt–Sn [18,19] imposes another fundamental limitation, in that nearly all annealed surfaces of Pt-rich alloys are strongly enriched (relative to the bulk) in Sn, the $Pt_3Sn(111)$ surface being the exception, e.g. even a solid-solution of 2 at% in Pt has an annealed surface composition of 20–25 at% Sn [14]. These thermodynamic limitations have not allowed us to vary the composition of Pt–Sn surfaces across the Pt-rich end in the way we were able to do with the Pt–Ru system [7]. From our experience with Pt–Ru alloys, the study of the variation in activity with surface concentration can be very powerful, revealing a great deal of information about the mechanism of action of the adatom, e.g. Ru or Sn. It is, therefore, fundamentally important to develop

* To whom correspondence should be addressed.

a new surface modification method which would allow one to create a continuous series of Pt–Sn surface alloys having compositions from 5 to 25 at% Sn. Such surface alloys may also be of technological interest.

Reported herein is a description of a surface modification technique for the preparation of polycrystalline Pt–Sn catalysts which might be used as an anode catalyst in fuel cells running on industrial hydrogen (contaminated with CO and other hydrocarbons) or on a hydrogen feed stream derived from steam-reforming carbon-based fuels. We describe here a novel metal ion implantation method we used to form non-equilibrium Pt–Sn surface alloy compositions that we were unable to form by classical metallurgy. We will present results for the electrooxidation of CO and CO/$H_2$ mixtures on a Pt–Sn surface alloy having $\sim$ 8.6 at% of Sn and compare the kinetics with that of the $Pt_3Sn(hkl)$ alloys studied previously.

## 2. Experimental

### 2.1. Implantation method

High-dose ion implantation of Sn into polycrystalline Pt was done using a relatively new kind of surface modification technique. In this method, the substrate (here Pt) is immersed in a plasma of the desired implantation species (here Sn) and repetitively pulse-biased to high negative voltage. A high voltage sheath rapidly forms at the plasma–substrate boundary, and plasma ions are accelerated through the sheath and into the substrate, thereby accomplishing implantation into the substrate of plasma ions at an energy determined by the bias voltage. This technique has been called plasma source (or plasma immersion) ion implantation, and has been developed by a number of groups, principally by Conrad and co-workers for the case of gaseous plasmas [20–22]. We have taken the method a step further by combining it with vacuum-arc-produced metal plasma techniques to provide for the implantation of metals [23,24]. The Sn plasma is produced by a vacuum arc discharge of the kind that has been extensively explored by many workers [25]. Droplet contamination from the plasma stream was removed by a "magnetic filter" configuration employing a curved magnetic duct which stops line-of-sight transmission of solid droplets while allowing transport of plasma along the curved axial magnetic field [25,26]. A pure and highly-ionized Sn plasma exits the filter and is directed towards the platinum substrate, which is repetitively pulse-biased (4 $\mu$s pulse and duty cycle 50%) for the duration of the plasma pulse (2 ms pulses at a repetition rate of 1 pulse every 2 s) to a negative voltage ($-2$ kV) that determines the ion implantation energy (about 3 kV, since the Sn ions are multiple-stripped with a mean charge state of about 1.5 [27,28]). The process is continued until the desired concentration of implanted Sn ions is accumulated. A simplified schematic of the set-up is shown in fig. 1.

### 2.2. UHV preparation and characterization

A detailed outline of alloy preparation and UHV characterization of $Pt_3Sn(hkl)$ alloys was reported previously [15]. In the present work, prior to electrochemical measurements, the implanted Pt sample (Pt–Sn(IMP)) was prepared by two different methods. The first of these methods involved cleaning of the Pt–Sn(IMP) entirely in UHV by the same sputtering (0.5 keV $Ar^+$)-annealing (650°C) cycles used for the $Pt_3Sn(hkl)$ alloys, which are repeated until only Pt and Sn are observed by Auger electron spectroscopy (AES). Although the annealing cycles are short (10 min) and at a temperature which is only about one-half the bulk melting point of $Pt_3Sn$, there is the possibility that there is precipitation of $Pt_3Sn$ nanocrystals in the near-surface region during these cycles. Thus, for comparison, a second procedure was used, in which the implanted sample was pre-cleaned chemically, then cleaned in UHV only by ion-bombardment. The Pt–Sn(IMP) sample was cleaned in an ultrasonic bath of 3 M KOH, then dipped briefly into 1 M $H_2SO_4$, rinsed in pyrolytically distilled water and, finally, transferred into the UHV chamber. It was found that the surface composition following ion-sputtering, as determined by low-energy ion scattering (LEIS) [15], was essentially identical for these two methods of preparation, as was the electrocatalytic activity. In this paper, only the results for the Pt–Sn(IMP) alloy prepared by the sputtering/annealing method are shown.

### 2.3. Electrochemical measurements

The UHV prepared alloy surfaces were mounted in a special rotating disk electrode arbor [29] and immersed

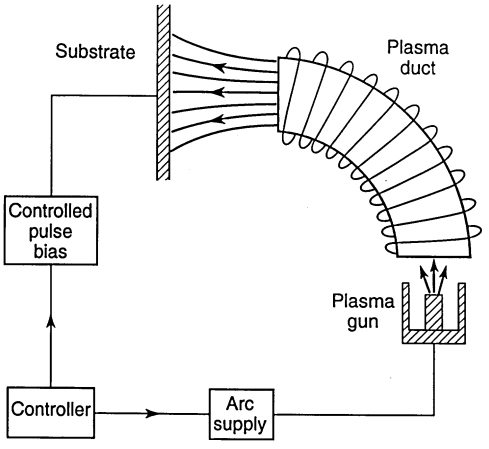


Fig. 1. Simplified schematic of the plasma immersion ion implantation apparatus.

in electrolyte under potential control at ~ 0.2 V in 0.5 M $H_2SO_4$ (Baker Ultrex). The electrolyte was prepared with triply pyrodistilled water and thermostated at 65°C, by circulating constant temperature bath connected with the water jacket of a standard three-compartment electrochemical cell. The reference electrode was a saturated calomel electrode (SCE) separated by a bridge from the reference compartment. All potentials in this paper are, however, referenced to the reversible hydrogen electrode potential (RHE) at the same temperature (calibrated from the hydrogen oxidation/reduction reaction on pure Pt). The CO/$H_2$ gas mixture as well as pure CO (6N $H_2$, 4N CO) were purchased from Matheson; the purity of the argon purge gas was 5N8 (Air Products). Data from the Pine Instrument bipotentiostat were acquired digitally on an IBM PC using Lab View for Windows.

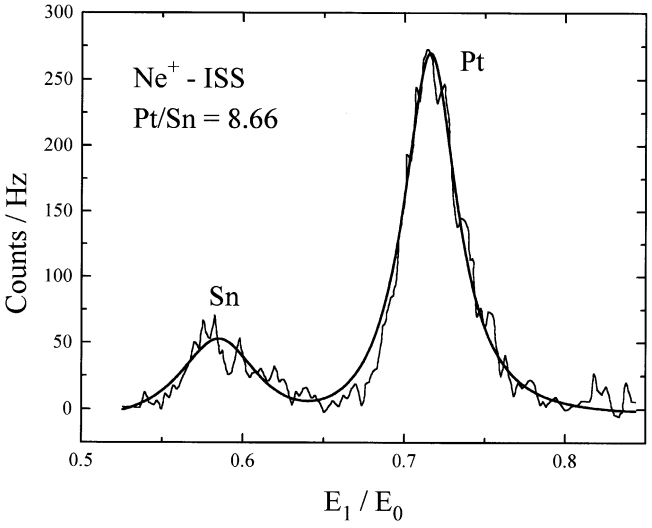


Fig. 2. Low-energy ion-scattering (LEIS) spectra for Pt–Sn(IMP) of the sputter-cleaned surface (0.5 keV $Ar^+$) of Pt–Sn(IMP); see ref. [30].

## 3. Results and discussion

As we noted recently, determination of the surface structure and the surface composition of bimetallic single-crystal surfaces by UHV spectroscopic techniques, in combination with the ability to transfer UHV prepared crystals to a classical rotating disk electrode (RDE) configuration without contamination, has yielded a wealth of information on the role of crystallographic structure and composition of $Pt_3Sn(hkl)$ in the electrooxidation of CO and CO/$H_2$ mixtures [14,15]. In order to compare the kinetics of electrooxidation of CO and CO/$H_2$ mixtures on the Pt–Sn(IMP) surface to other Pt–Sn systems, representative results for $Pt_3Sn(hkl)$ alloys from previous work are presented along with the new data for Pt–Sn(IMP).

### *3.1. Surface composition of Pt–Sn(IMP)*

After a few sputter/anneal cycles, a surface that is perfectly clean by AES was obtained. The normal incident LEIS spectrum following the final sputter is shown in fig. 2. Using the theoretical ion-scattering cross-sections [30] for Sn and Pt, which we used in our study of $Pt_3Sn$, the composition of the Pt–Sn(IMP) surface is ~ 8.6 at% Sn after this pre-treatment schedule. Because of some selective sputtering of Sn, the subsurface concentration is probably slightly higher than 8.6 at% Sn, but the previous results with $Pt_3Sn$ indicate that with our sputtering conditions the selectivity factor is rather small. For future studies, non-equilibrium surface concentrations between 8.6 and 25 at% will be obtained directly by higher doses of implanted Sn. While the 8.6 at% Sn surface is thermally metastable, i.e. the surface becomes enriched in Sn upon thermal annealing, there appears to be a kinetic stabilization of this surface composition at the temperatures relevant to polymer electrolyte fuel cells, e.g. < 100°C. The electrocatalytic activity of the surface was found to be very stable over the time period of the electrochemical measurements, e.g. typically 2–4 h at 60°C. A depth profile analysis by ion beam etching combined with LEIS indicated the Sn concentration is essentially constant to a depth of about 5 nm.

### *3.2. Cyclic voltammetry and $H_2$ oxidation on Pt–Sn(IMP)*

The corresponding base voltammetry for the Pt–Sn(IMP) electrode and the polarization curves in $H_2$-saturated electrolyte are shown in figs. 3a and 3b, respectively; these curves were recorded immediately following transfer from UHV to argon purged 0.5 M $H_2SO_4$. The cyclic voltammogram of the Pt–Sn(IMP) electrode is significantly different from that of a clean polycrystalline Pt pre-treated in the same way even though only 8.6 at% of Sn is present on the surface. The charge associated with the hydrogen adsorption (in potential region $0.1 < E < 0.4$ eV) is still close to 200 $\mu C/cm^2$, about what one would expect based on the Pt vs. Sn surface atomic ratio assuming that hydrogen is adsorbed only on Pt sites [14,15]. But the distribution of the charge in potential is very different from pure Pt, particularly the lack of two or more distinct peaks. Since these distinct peaks are now known [31] to be associated with the desorption/adsorption of (bi)sulfate concomitant with hydrogen adsorption/desorption, their absence on the Pt–Sn(IMP) surface implies that the presence of Sn in the surface, even at only 8.6 at%, affects anion adsorption more than hydrogen adsorption.

After recording the cyclic voltammogram, the electrolyte was saturated with $H_2$ and the hydrogen oxidation currents were recorded at different rotation rates, as shown in fig. 3b. Considering that the surface concentration of Pt is high and that the hydrogen reaction on Pt in acid solutions is one of the fastest known electrochemi-

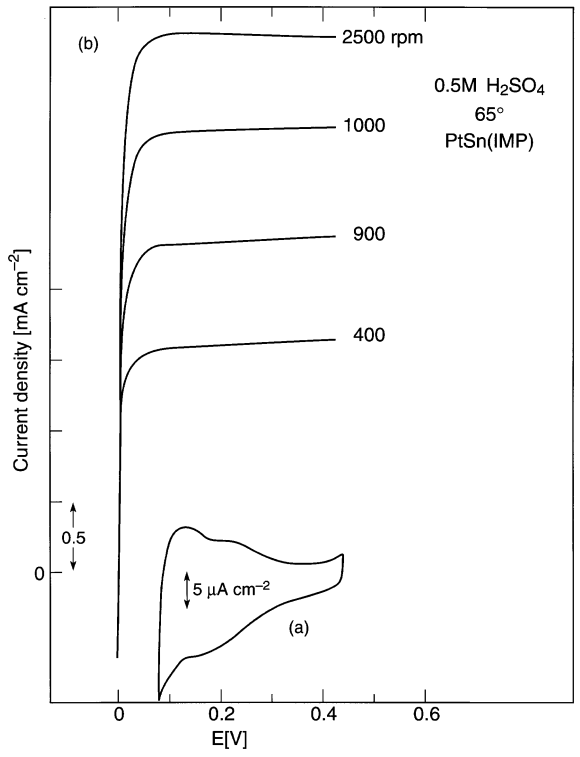


Fig. 3. (a) Cyclic voltammogram of the sputtered Pt–Sn(IMP) sample in the RDE assembly after transfer from UHV; 0.5 M $H_2SO_4$ purged with argon, 65°C; 20 mV/s. (b) $H_2$ oxidation on the Pt–Sn(IMP) electrode in 0.5 M $H_2SO_4$ purged with hydrogen; 65°C; 20 mV/s.

cal reactions, it is not surprising that the polarization curves for the oxidation of hydrogen, fig. 3b, are almost identical with the oxidation of hydrogen on pure Pt in 0.5 M $H_2SO_4$ [13]. From an analysis of $i^{-1}$ vs. $\omega^{-0.5}$ plots (not shown), based on the discussion in ref. [13], the minimum value of the exchange current density for the oxidation of molecular $H_2$ is $\sim$ 50–60 mA/cm$^{-2}$, equivalent to a turnover number of $\geqslant$100 molecules of hydrogen per Pt atoms per second (at equilibrium). While Sn may have some effect (unmeasurable by standard RDE methods) on the $H_2/H^+$ kinetics, the rate remains extremely high and the Pt–Sn(IMP) surface behaves as a completely reversible $H_2/H^+$ electrode.

### 3.3. Electrooxidation of CO and CO/Ar mixtures at 65°C; Pt–Sn(IMP) vs. $Pt_3Sn(hkl)$

#### 3.3.1. Electrooxidation of CO

As outlined in the Introduction and reported in ref. [15], the mechanism for CO oxidation on $Pt_3Sn(hkl)$ appears to be consistent with a bifunctional action by the two metals. It was proposed that at a saturation coverage of $CO_{ad}$ on Pt sites two different states of $CO_{ad}$ are present at the surface; strongly adsorbed $CO^s_{ad}$, a spectator during the CO electrooxidation at low overpotentials, and weakly adsorbed $CO^w_{ad}$, i.e., an active species which at low overpotential reacts with an oxygenated species adsorbed on Sn atoms through a Langmuir–Hinshelwood type reaction:

$$CO^w_{ad} + OH_{ad} \xrightarrow{rds} CO_2 + H^+ + e^- \qquad (1)$$

We also proposed that the weakly adsorbed state $CO^w_{ad}$ on $Pt_3Sn(hkl)$ is a consequence of strong intermetallic bonding in this alloy, and, considering that CO only adsorbs on Pt sites of a Pt–Sn alloy, we suggested that the structural density of the CO electrooxidation reaction on $Pt_3Sn(hkl)$ surfaces appears to be due primarily to a higher mobility of $CO^w_{ad}$ and higher fraction of the $CO_{ad}$ in the weakly bonded state on the (111) surface relative to the (110) surface [15], and not due to the small difference in Sn surface composition. On both $Pt_3Sn(111)$ and $Pt_3Sn(110)$, however, a relatively high pressure of CO is needed to populate the weakly adsorbed state, affecting a positive reaction order with respect to the concentration of CO in solution.

In the following, we compare the kinetics of CO oxidation on the sputtered $Pt_3Sn(110)$ surface (21 at% Sn in surface) with the kinetics on the implanted Pt–Sn(IMP) near-surface alloy. $Pt_3Sn(110)$ was chosen as the basis for comparison in order to separate structural effects from surface composition effects; it is our experience that in many electrocatalytic processes on Pt(*hkl*) surfaces the (110) surface is the closest in activity to a polycrystalline sample. The polarization curve for the oxidation of pure CO on $Pt_3Sn(111)$ alloy is only shown to give an idea of the magnitude of the structural effects in this system (which are quite substantial). The polarization curves at 2500 rpm for the electrooxidation of pure CO and two CO/Ar mixtures on $Pt_3Sn(110)$ are shown in fig. 4a. In order to closely approach the steady-state activity these measurements were made at the slow sweep rate of 1 mV/s. Under these conditions, the diffusion-limiting current densities for the oxidation of CO in these three gases are 2.33, 0.58, and 0.05 mA/cm$^2$, respectively, so that mass-transfer resistances are negligible for current densities below $\sim$ 0.5, 0.2, and 0.01 mA/cm$^2$, respectively. For $Pt_3Sn(110)$, kinetically-controlled current densities ($i_k$) occur below 0.3 V. Quite clearly the measurements with the CO/Ar mixture did establish a positive reaction order ($m$) with respect to CO (see insert in fig. 4a with $m \approx 0.25$. In contrast, the reaction order on Pt and Pt–Ru alloys is negative [13], $-0.2$ to $-0.5$, the difference arising from the absence of the weakly bound state of $CO^w_{ad}$ on these surfaces. Fig. 4b shows potentiodynamic oxidation curves for the electrooxidation of pure CO, 15% CO/Ar and 2% CO/Ar on Pt–Sn(IMP) under the same conditions as in fig. 4a. Fig. 4b reveals that a reduced partial pressure of CO (i.e., its dilution with argon) indeed produces a negative potential shift in the onset of CO oxidation, consistent with a positive reaction order; the $\log i_k$ vs. $\log P_{CO}$ plots, shown in the insert in fig. 4b, confirm that the reaction order is close to 0.25. A comparison of figs. 4a and 4b clearly shows that the activity of $Pt_3Sn(110)$ alloy and the Pt–Sn(IMP)

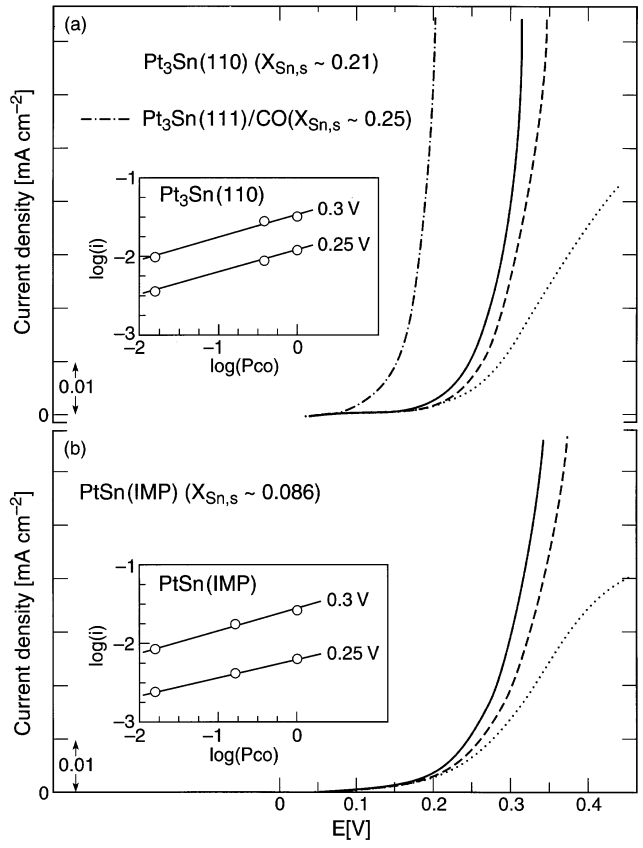


Fig. 4. (a) Polarization curves for oxidation of pure CO (——), 25% CO/Ar (– – –) and 2% CO/Ar (· · ·) mixtures on a sputter-cleaned $Pt_3Sn(110)$. (b) Polarization curves for oxidation of pure CO (——), 15% CO/Ar (– – –) and 2% CO/Ar (· · ·) mixture on a sputter-cleaned Pt–Sn(IMP) electrode. Inserts in (a) and (b) show a reaction order for CO oxidation on $Pt_3Sn(110)$ and Pt–Sn(IMP). Polarization curve for oxidation of pure CO (– · –) on an annealed $Pt_3Sn(111)$ electrode shown as indication of the magnitude of structure effects in this system. 0.5 M $H_2SO_4$ at 65°C. Sweep rate, 1 mV/s, Rotation rate, 2500 rpm.

surface is almost identical. However, the surface composition of Sn on the sputtered (110) surface is different than on Pt–Sn(IMP), i.e., 21% versus 8.6%, respectively. This indicates that an optimum surface composition for a polycrystalline Pt–Sn alloy might be found in the range $\sim 10 < \chi_{Sn,s} < 25$ at%, exactly in the composition region where there is no bulk alloy phase. We believe that the optimum surface composition should not exceed 25 at% Sn because the onset potential for CO oxidation on the annealed $Pt_3Sn(110)$ alloy with the surface composition, $\chi_{Sn,s} \approx 53$ at%, is $\sim 0.15$ eV lower than for the sputtered surface with $\chi_{Sn,s} \approx 21$ at%. Thus, by utilizing the implantation technique one can indeed create new Pt–Sn surfaces with non-equilibrium compositions that may prove to be uniquely active. Equally importantly, by examining the change in activity with surface composition across this region, we can learn a great deal more about the mechanism of action of Sn, as in this composition region the various Pt–Sn ensembles, e.g. Pt–Sn pairs, Sn atoms with Sn in the second coordination shell, etc., distribution function (ideally) change dramatically.

### 3.3.2. Electrooxidation of 2% CO/$H_2$ mixtures

A 2% CO/$H_2$ mixture is the most common hydrogen feed stream for a low-temperature fuel cell which uses a hydrocarbon as the primary fuel; this mixture is produced by steam reforming and shifting [10]. In order to separate the structural effects from the surface composition effects, the oxidation of CO/$H_2$ mixture will be compared on the Pt–Sn(IMP) surface and $Pt_3Sn(110)$ alloy; as in the case of CO oxidation, the electrocatalytic activity of $Pt_3Sn(111)$ is only included as cross-reference. Fig. 5 shows the quasi-steady state (1 mV/s) oxidation of 2% CO/$H_2$ on three different Pt–Sn alloys at 2500 rpm. In order to ensure the equilibration of the electrode surfaces with CO prior to the recording of the oxidation current, the electrode potential in all of the following experiments was held at 0.05 V (the immersion potential) for 3 min at a rotation rate of 2500 rpm. Under these conditions, the diffusion-limiting current density for the oxidation of pure $H_2$ is 4.04 mA/cm$^2$ [13], so that mass-transport resistances are negligible below $\sim 0.5$ mA/cm$^2$. The $Pt_3Sn(111)$ surface exhibits the lowest overpotential for the oxidation of $H_2$ in the presence of 2% CO, shifted negatively by $\sim 0.1$ eV relative to either $Pt_3Sn(110)$ or Pt–Sn(IMP). The insert in fig. 3 is a magnification of the low current density region were all currents are kinetically controlled. As with the oxidation

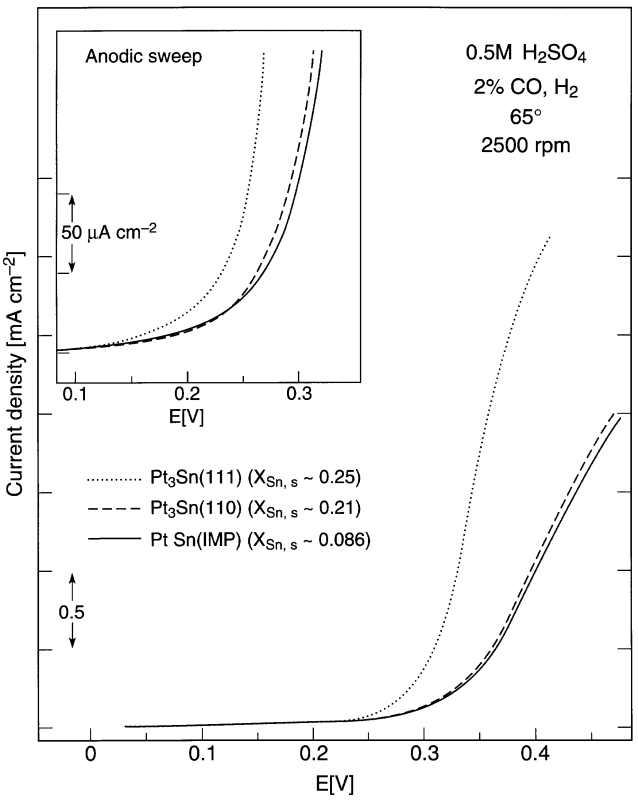


Fig. 5. Current–potential curves recorded on sputter-cleaned $Pt_3Sn(110)$, annealed $Pt_3Sn(111)$ and sputter-cleaned Pt–Sn(IMP) electrodes in 0.5 M $H_2SO_4$ saturated with a 2% CO in $H_2$ mixture at rotation rate of 2500 rpm. Sweep rate, 1 mV/s. Temperature, 65°C.

of pure CO, $Pt_3Sn(110)$ and Pt–Sn(IMP) surfaces have essentially identical activity for the oxidation of $H_2$ in the presence of 2% CO.

## 4. Conclusions

It may be concluded that an ion implantation technique has been developed for the modification of a Pt substrate by Sn. This method is used to create a non-equilibrium Pt–Sn(IMP) near-surface alloy with ca. 8.6 at% Sn. The kinetics of the electrooxidation of CO and a 2% CO/$H_2$ mixture on Pt–Sn(IMP) is essentially identical to that of $Pt_3Sn(110)$. The fact that any non-equilibrium composition can be easily prepared by this implantation method opens an interesting practical opportunity to create a new Pt–Sn alloy fuel cell catalyst having an otherwise unobtainable surface composition of Sn. This method also appears to have general utility in alloy catalysis as a means of exploring compositions in thermodynamically unfavorable regions of the bulk phase diagram.

## Acknowledgement

We are indebted to Hubert Gasteiger for his contribution to all of the $Pt_3Sn$ single crystal work. We would also like to thank Lee Johnson and Frank Zucca for their invaluable help in polishing the $Pt_3Sn$ single crystals and in the setting up of the experimental apparatus. This work was jointly funded by the Office of Energy Research and by the Office of Transportation Technologies of the US Department of Energy under Contract No. DE-AC03-76SF00098.

## References

[1] B. McNicol, J. Electroanal. Chem. 18 (1981) 71, and references therein.
[2] D.W. McKee and A.J. Scarpellino, Electrochem. Technol. 6 (1968) 101;
L.W. Niedrach, D.W. McKee, J. Paynter and I.F. Danzig, Electrochem. Technol. 4 (1967) 318.
[3] R. Parsons and T. Van der Not, J. Electroanal. Chem. 257 (1988) 9.
[4] P.N. Ross, K. Kinoshita, A.J. Scarpellino and P. Stonehart, J. Electroanal. Chem. 63 (1975) 97; 59 (1975) 177.
[5] S. Motoo and T. Okada, J. Electroanal. Chem. 157 (1983) 139.
[6] M. Watanabe, M. Shibata and S. Motoo, J. Electroanal. Chem. 187 (1985) 161.
[7] H.A. Gasteiger, N. Marković, P.N. Ross Jr. and E.J. Cairns, J. Phys. Chem. 98 (1994) 617.
[8] R. Ianniello, V.M. Schmidt, U. Stimming, J. Stumper and A. Wallau, Electrochim. Acta 39 (1994) 1863.
[9] T. Iwasita, R. Dalbeck, E. Pastor and X. Xia, Electrochim. Acta 39 (1994) 1817.
[10] H.S. Murray, in: *Fuel Cell*, 1985 Fuel Cell Seminar, Book of Abstracts, sponsored by the National Fuel Cell Coordinating Group, Tucson, May 1985, p. 129.
[11] H.A. Gasteiger, N. Marković, P.N. Ross Jr. and E.J. Cairns, Electrochim. Acta 39 (1994) 1825.
[12] N.M. Marković, H.A. Gasteiger, P.N. Ross Jr., X. Jiang, I. Villegas and M.J. Weaver, Electrochim. Acta 40 (1995) 91.
[13] H.A. Gasteiger, N. Marković and P.N. Ross, J. Phys. Chem. 99 (1995) 8290.
[14] H.A. Gasteiger, N.M. Marković and P.N. Ross Jr., J. Phys. Chem. 99 (1995) 8945.
[15] H.A. Gasteiger, N. Marković and P.N. Ross Jr., Catal. Lett. 36 (1996) 1.
[16] A.B. Anderson, E. Grantscharova and P. Schiller, J. Electrochem. Soc. 142 (1995) 1880.
[17] M. Hansen, *Constitution of Binary Alloys* (McGraw-Hill, New York, 1958).
[18] A.N. Haner, P.N. Ross and U. Bardi, Catal. Lett. 8 (1991) 1.
[19] A.N. Haner, P.N. Ross and U. Bardi, Surf. Sci. 249 (1991) 15.
[20] J.R. Conrad, J.L. Radtke, R.A. Dodd, F.J. Worzala and N.C. Tran, J. Appl. Phys. 62 (1987) 4591.
[21] J.T. Scheuer, M. Shamine and J.R. Conrad, J. Appl. Phys. 67 (1990) 1241.
[22] *Proc. First Int. Workshop on Plasma-Based Ion Implantation*, J. Vac. Sci. Technol. B 12 (1994) pp. 815–998.
[23] I.G. Brown, X. Godechot and K.M. Yu, J. Appl. Phys. Lett. 58 (1991) 1392.
[24] I.G. Brown, A. Anders, S. Anders, M.R. Dickinson, R.A. MacGill, O.R. Monteiro, E.M. Oks, S. Raoux, Z. Wang and G. Yushkov, Mater. Res. Symp. Proc. 396 (1996) 467.
[25] R.L. Boxman, P. Martin and D. Sanders, eds., *Vacuum Arc Science and Technology* (Noyes, New York, 1995).
[26] A. Anders, S. Anders and I.G. Brown, Plasma Sources Sci. Technol. 4 (1995) 1.
[27] I.G. Brown and X. Godechot, IEEE Trans. Plasma Sci. PS-19 (1991) 713.
[28] I.G. Brown, Rev. Sci. Instr. 65 (1994) 3061.
[29] N.M. Marković, H.A. Gasteiger and P.N. Ross Jr., J. Phys. Chem. 99 (1995) 3411.
[30] H.A. Gasteiger, P.N. Ross Jr. and E.J. Cairns, Surf. Sci. 99 (1993) 8290.
[31] N. Marković and P.N. Ross Jr., J. Electroanal. Chem. 330 (1992) 499.